


Isometric tensor network optimization for extensive Hamiltonians is free of barren plateaus

Qiang Miao and Thomas Barthel

*Department of Physics, Duke University, Durham, North Carolina 27708, USA
and Duke Quantum Center, Duke University, Durham, North Carolina 27701, USA* (Received 23 May 2023; accepted 15 April 2024; published 14 May 2024)

We explain why and numerically confirm that there are no barren plateaus in the energy optimization of isometric tensor network states (TNS) for extensive Hamiltonians with finite-range interactions, which are, for example, typical in condensed matter physics. Specifically, we consider matrix product states (MPS) with open boundary conditions, tree tensor network states (TTNS), and the multiscale entanglement renormalization ansatz (MERA). MERA are isometric by construction, and for the MPS and TTNS, the tensor network gauge freedom allows us to choose all tensors as partial isometries. The variance of the energy gradient, evaluated by taking the Haar average over the TNS tensors, has a leading system-size independent term and decreases according to a power law in the bond dimension. For a hierarchical TNS (TTNS and MERA) with branching ratio b , the variance of the gradient with respect to a tensor in layer τ scales as $(b\eta)^\tau$, where η is the second largest eigenvalue of a Haar-average doubled layer-transition channel and decreases algebraically with increasing bond dimension. The absence of barren plateaus substantiates that isometric TNS are a promising route for an efficient quantum-computation-based investigation of strongly correlated quantum matter. The observed scaling properties of the gradient amplitudes bear implications for efficient TNS initialization procedures.

DOI: [10.1103/PhysRevA.109.L050402](https://doi.org/10.1103/PhysRevA.109.L050402)

Introduction. Rapid advances in quantum technology have opened new routes for the solution of hard quantum-matter ground-state problems [1]. An important approach are variational quantum algorithms (VQA) [2], in which classical optimization is performed on parametrized quantum circuits. Numerous studies successfully applied VQA to few-body systems, but applications of generic unstructured or overly expressive VQA to many-body systems face multiple challenges: the limited number of qubits and gate fidelities, convergence to local minima [3–6], and so-called barren plateaus, where gradient amplitudes and cost-function variations decay exponentially in the size of the simulated system [7–10]. VQA with barren plateaus are not trainable as the inability to precisely estimate exponentially small gradients with quantum measurements will result in random walks on the flat landscape. The barren plateau problem can be resolved if an initial guess close to the optimum and specific optimization strategies are available [11–21], but such resolutions are not universal [22].

Unstructured circuits like the hardware efficient ansatz and brickwall circuits must be deep to cover relevant parts of the Hilbert space [23–25]. The high expressiveness of such circuits [26–28] can be seen as the source for the barren plateaus [29]. The latter can be motivated by typicality properties [30,31] of such states [32–34]. So, it is generally preferable to work with more structured and less entangled classes of states that are adapted to the particular optimization problem in order to balance expressiveness and trainability.

In this Letter, we demonstrate that VQA barren plateaus can be avoided for quantum many-body ground-state problems by employing matrix product states (MPS) with open boundary conditions [35,37–42], tree tensor network states

(TTNS) [43–47], or the multiscale entanglement renormalization ansatz (MERA) [48–50]. We refer to these tensor network states (TNS) as being *isometric* because all tensors in the network are either isometries by definition (MERA) or one can use the TNS gauge freedom [36,51] to make all tensors isometric (MPS and TTNS). The entanglement structures of these TNS are well adapted to those in many-body ground states, and classical simulations established TNS algorithms as valuable tools for the investigation of strongly correlated quantum matter. However, the classical TNS computation costs grow quickly with increasing TNS bond dimension χ which controls the achievable approximation accuracy. Especially for two-dimensional (2D) and three-dimensional (3D) systems, the rapid growth of classical tensor contraction costs in χ [52] limits investigations of important phenomena such as high-temperature superconductivity and topological order.

Fortunately, variations of isometric TNS can be implemented on quantum computers [52–56], which may allow us to substantially reduce computation costs in comparison to classical simulations [52,57]. Recently, barren plateaus have been studied using graph techniques for MPS [58,59] and ZX calculus for TNS with bond dimension $\chi = 2$ [60,61] in the energy optimization for (tensor products of) single-site Hamiltonians. Of course, such ground-state problems are actually solved by (products of) the single-site ground states and, hence, are of no practical relevance [62].

Here, we address the actual (QMA-complete [63–67]) ground-state problem for extensive translation-invariant Hamiltonians

$$\hat{H} = \sum_i \hat{h}_i \quad \text{with} \quad \text{Tr} \hat{h}_i = 0 \quad (1)$$

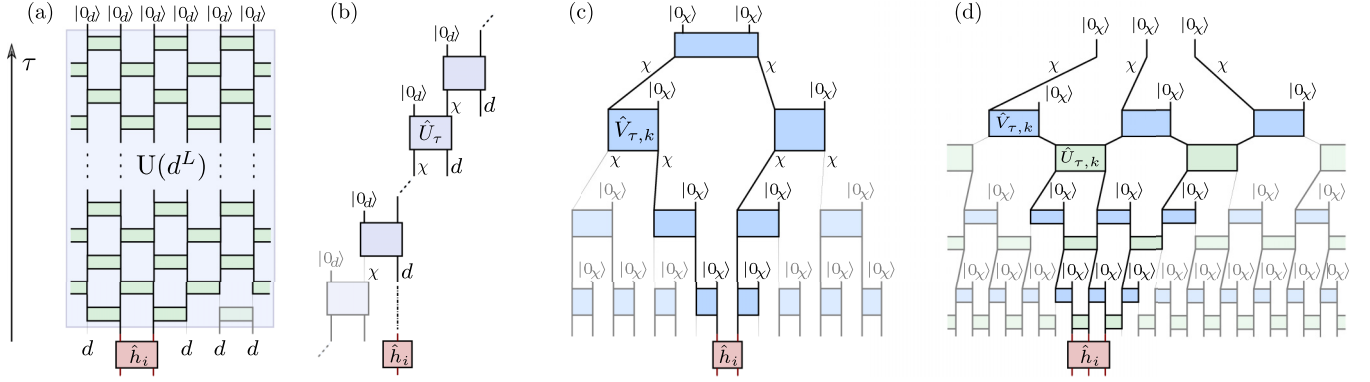


FIG. 1. Isometric quantum circuits. (a) A generic brickwall quantum circuit for L qudits consisting of layers of nearest-neighbor two-qudit gates. (b) MPS quantum circuit with single-site Hilbert space dimension d and bond dimension χ . Using the TNS gauge freedom to bring the MPS into left-canonical form [35,36], the expectation value $\langle \Psi | \hat{h}_i | \Psi \rangle$ for an operator acting on site i only depends on the tensors for sites $\tau \geq i$. (c), (d) Binary 1D TTNS and MERA quantum circuits with branching ratio $b = 2$ and bond dimension χ . Only the nonshaded tensors can influence the expectation values of the local operator \hat{h}_i and constitute its *causal cone*.

encountered in quantum many-body physics, where the finite-range interaction term \hat{h}_i acts nontrivially in the vicinity of site i . We explain why the corresponding VQA, minimizing the energy expectation value $\langle \Psi | \hat{H} | \Psi \rangle$ with respect to an isometric TNS $|\Psi\rangle$, does *not* encounter barren plateaus. Detailed proofs of the analytical results are given in Ref. [68] and they are confirmed here numerically.

The key ideas are the following. Due to the isometric properties of the tensors, the TNS expectation value for a local interaction term \hat{h}_i only depends on tensors in the causal cone of \hat{h}_i . The expectation values can be evaluated by propagating causal-cone density operators $\hat{\rho}$ in the preparation direction (decreasing τ in Fig. 1) with transition maps \mathcal{M} and/or interaction terms \hat{h} in the renormalization direction (increasing τ) with \mathcal{M}^\dagger . To evaluate the variance of the energy gradient for TNS tensors sampled according to the Haar measure, doubled transition quantum channels $\mathcal{E}^{(2)} := \text{Avg } \mathcal{M} \otimes \mathcal{M}$ are applied multiple times to $\hat{\rho} \otimes \hat{\rho}$ and their adjoints $\mathcal{E}^{(2)\dagger}$ to $\hat{h} \otimes \hat{h}$. While the image of $\hat{\rho} \otimes \hat{\rho}$ will quickly converge to a unique steady state, we find that the leading contribution from $\hat{h} \otimes \hat{h}$ has a decay factor $(b\eta)^\tau$, where η is the second largest eigenvalue of $\mathcal{E}^{(2)}$ and b the branching ratio of the TNS ($b = 1$ for MPS and $b > 1$ for TTNS and MERA).

This leads to three key observations. For isometric TNS and extensive Hamiltonians with finite-range interactions (i) the gradient variance is independent of the system size rather than exponentially small, (ii) the gradient variance for a tensor in layer τ of hierarchical TNS decays exponentially in the layer index τ , and (iii) the gradient variances decrease according to power laws in the TNS bond dimension χ . Instead of Euclidean gradients in parametrized quantum circuits, we employ Riemannian gradients which greatly simplifies the proofs [68].

Riemannian TNS Gradients. All tensors in the considered isometric TNS are either unitaries \hat{U} or partial isometries $\hat{V} : \mathbb{C}^{N_1} \rightarrow \mathbb{C}^{N_1} \otimes \mathbb{C}^{N_2}$ with $\hat{V}^\dagger \hat{V} = \mathbb{1}_{N_1}$; MERA are isometric by definition [48]; the MPS and TTNS can always be brought into isometric form by using the TNS gauge freedom [35,36,51]. The isometries \hat{V} can be implemented as partially

projected unitaries in the form

$$\hat{V} = \hat{U} (\mathbb{1}_{N_1} \otimes |0_{N_2}\rangle) \quad \text{with} \quad \hat{U} \in \text{U}(N_1 N_2) \quad (2)$$

and an arbitrary reference state $|0_{N_2}\rangle \in \mathbb{C}^{N_2}$. The TNS energy expectation values can be written in the form

$$E(\hat{U}) = \langle \Psi(\hat{U}) | \hat{H} | \Psi(\hat{U}) \rangle = \text{Tr}(\hat{X} \hat{U}^\dagger \hat{Y} \hat{U}), \quad (3)$$

where we explicitly denote the dependence on one of the TNS unitaries $\hat{U} \in \text{U}(N)$ and $\hat{U} := \hat{U} \otimes \mathbb{1}_M$. The Hermitian operators \hat{X} and \hat{Y} depend on the other TNS tensors and \hat{Y} also comprises the Hamiltonian. The Riemannian energy gradient is then given by [52,68–71]

$$\hat{g}(\hat{U}) = \partial_{\hat{U}} \langle \Psi | \hat{H} | \Psi \rangle = \text{Tr}_M(\hat{Y} \hat{U} \hat{X} - \hat{U} \hat{X} \hat{U}^\dagger \hat{Y} \hat{U}). \quad (4)$$

Averaged according to the Haar measure, \hat{g} vanishes,

$$\text{Avg}_{\hat{U}} \hat{g} := \int dU \hat{g}(\hat{U}) = \frac{1}{2} \int dU [\hat{g}(\hat{U}) + \hat{g}(-\hat{U})] = 0.$$

To assess the question of barren plateaus, the Haar variance of the Riemannian gradient (4) can be quantified by

$$\text{Var}_{\hat{U}} \hat{g} := \text{Avg}_{\hat{U}} \frac{1}{N} \text{Tr}(\hat{g}^\dagger \hat{g}). \quad (5)$$

We can expand \hat{g} in an orthonormal basis of N^2 Hermitian and unitary operators $\{\hat{\sigma}_n\}$ with $\hat{\sigma}_n^2 = \mathbb{1}_N$ such that $\hat{g} = i\hat{U} \sum_{n=1}^{N^2} \alpha_n \hat{\sigma}_n / N$. On a quantum computer, the rotation-angle derivatives can be determined as energy differences [52,71]

$$\alpha_n = E(\hat{U} e^{i\pi \hat{\sigma}_n / 4}) - E(\hat{U} e^{-i\pi \hat{\sigma}_n / 4}). \quad (6)$$

Equation (5) then agrees with the variance $\int dU \frac{1}{N^2} \sum_n \alpha_n^2$ of rotation-angle derivatives, motivating the employed factor $1/N$.

We focus on extensive Hamiltonians (1) with finite-range interactions \hat{h}_i . Let τ identify one unitary tensor \hat{U}_τ in the TNS and \mathcal{S}_τ the set of physical sites i with \hat{U}_τ in the causal cone (cf. Fig. 1). The gradient (4) then takes the form

$$\hat{g}(\hat{U}_\tau) = \sum_{i \in \mathcal{S}_\tau} \hat{g}_\tau^{(i)} \quad \text{with} \quad \hat{g}_\tau^{(i)} := \partial_{\hat{U}_\tau} \langle \Psi | \hat{h}_i | \Psi \rangle. \quad (7)$$

Averaging over all unitaries of the TNS, the Haar variance of $\hat{g}(\hat{U}_\tau)$ reads

$$\text{Var} \hat{g}(\hat{U}_\tau) = \sum_{i_1, i_2 \in \mathcal{S}_\tau} \text{Avg} \frac{1}{N} \text{Tr} (\hat{g}_\tau^{(i_1)\dagger} \hat{g}_\tau^{(i_2)}), \quad (8)$$

where Avg denotes the Haar average over all remaining TNS tensors besides \hat{U}_τ .

Matrix Product States. Consider MPS of bond dimension χ for a system of L sites and single-site Hilbert-space dimension d ,

$$|\Psi\rangle = \sum_{s_1, \dots, s_L=1}^d \langle 0 | \hat{V}_1^{s_1} \hat{V}_2^{s_2} \dots \hat{V}_L^{s_L} | 0 \rangle |s_1, s_2, \dots, s_L\rangle. \quad (9)$$

Using its gauge freedom, the MPS can be brought to left-canonical (a.k.a. left-orthonormal) form [35,36], where the tensors \hat{V}_τ with $\langle a, s_\tau | \hat{V}_\tau | b \rangle := \langle a | \hat{V}_\tau^{s_\tau} | b \rangle$, $s_\tau = 1, \dots, d$, and $a, b = 1, \dots, \chi$ are isometries in the sense that $\hat{V}_\tau^\dagger \hat{V}_\tau = \mathbb{1}_\chi$. We use Eq. (2) to express them in terms of unitaries with $\hat{V}_\tau := \hat{U}_\tau (\mathbb{1}_\chi \otimes |0_d\rangle)$ in the bulk of the system such that $\hat{U}_\tau \in \text{U}(\chi d)$ [68].

For simplicity, let us first address Hamiltonians (1) with single-site terms $\hat{h}_i = \mathbb{1}_d^{\otimes(i-1)} \otimes \hat{h} \otimes \mathbb{1}_d^{\otimes(L-i)}$. Due to the left-orthonormality, the local expectation value $\langle \Psi | \hat{h}_i | \Psi \rangle$ is independent of all tensors \hat{U}_τ with $\tau < i$ such that $\mathcal{S}_\tau = \{1, \dots, \tau\}$. As we chose $\text{Tr} \hat{h} = 0$ without loss of generality, all off-diagonal contributions with $i_1 \neq i_2$ in Eq. (8) vanish. It remains to evaluate the diagonal contributions with $i_1 = i_2 = i \leq \tau$: The expectation value has the form (3). In particular,

$$\langle \Psi | \hat{h}_i | \Psi \rangle = \text{Tr} (\hat{X}_\tau^{(i)} \hat{U}_\tau^\dagger \hat{Y}_\tau^{(i)} \hat{U}_\tau) \quad \text{with} \quad (10a)$$

$$\hat{X}_\tau^{(i)} = \mathcal{M}_{\tau+1} \circ \dots \circ \mathcal{M}_L(|0\rangle\langle 0|) \otimes |0_d\rangle\langle 0_d|, \quad \text{and} \quad (10b)$$

$$\hat{Y}_\tau^{(i)} = \mathcal{M}_{\tau-1}^\dagger \circ \dots \circ \mathcal{M}_{i+1}^\dagger (\hat{L}^{(i)} \otimes \mathbb{1}_d), \quad (10c)$$

where $\hat{L}^{(i)} = \hat{V}_i^\dagger [\mathbb{1}_\chi \otimes \hat{h}] \hat{V}_i$, and we have defined the site-transition map (quantum channel)

$$\mathcal{M}_t(\hat{R}) := \sum_{s=1}^d \hat{V}_t^s \hat{R} \hat{V}_t^{s\dagger}. \quad (11)$$

According to Eq. (4), the contribution $\text{Avg} \text{Tr} (\hat{g}_\tau^{(i)\dagger} \hat{g}_\tau^{(i)})$ to the gradient variance (8) is quadratic in both $\hat{X}_\tau^{(i)}$ and $\hat{Y}_\tau^{(i)}$. The essential step is hence to evaluate the Haar averages $\text{Avg} \hat{X}_\tau^{(i)} \otimes \hat{X}_\tau^{(i)}$ and $\text{Avg} \hat{Y}_\tau^{(i)} \otimes \hat{Y}_\tau^{(i)}$, i.e.,

$$\text{Avg} \mathcal{M}_{\tau+1}^{\otimes 2} \circ \dots \circ \mathcal{M}_L^{\otimes 2}(|0, 0\rangle\langle 0, 0|), \quad \text{and} \quad (12)$$

$$\text{Avg} \mathcal{M}_{\tau-1}^{\dagger \otimes 2} \circ \dots \circ \mathcal{M}_{i+1}^{\dagger \otimes 2}(\hat{L}^{(i)} \otimes \hat{L}^{(i)}). \quad (13)$$

Taking the Haar average of $\mathcal{M}_t^{\otimes 2}$ over the corresponding unitary \hat{U}_t with $t \in \{\tau+1, \dots, L\}$ and $t \in \{i+1, \dots, \tau-1\}$, respectively, yields the doubled site-transition channel

$$\mathcal{E}_{\text{mps}}^{(2)} := \text{Avg}_{\hat{U}_t} \mathcal{M}_t^{\otimes 2} = |\hat{r}_1\rangle\langle\langle \mathbb{1}_{\chi^2} | + \eta_{\text{mps}} |\hat{r}_2\rangle\langle\langle \hat{\ell}_2 |. \quad (14)$$

Here, we have already written its diagonalized form, using a super-bra-ket notation for operators based on the Hilbert-Schmidt inner product $\langle\langle \hat{A} | \hat{B} \rangle\rangle := \text{Tr}(\hat{A}^\dagger \hat{B})$. The left and right eigenvectors are biorthogonal, $\langle\langle \hat{\ell}_i | \hat{r}_j \rangle\rangle = \delta_{i,j}$. The diagonalization shows that $\mathcal{E}_{\text{mps}}^{(2)}$ only has the two nonzero eigenvalues 1 and $\eta_{\text{mps}} = \frac{1-1/\chi^2}{d-1/(\chi^2 d)}$ with the corresponding unique steady

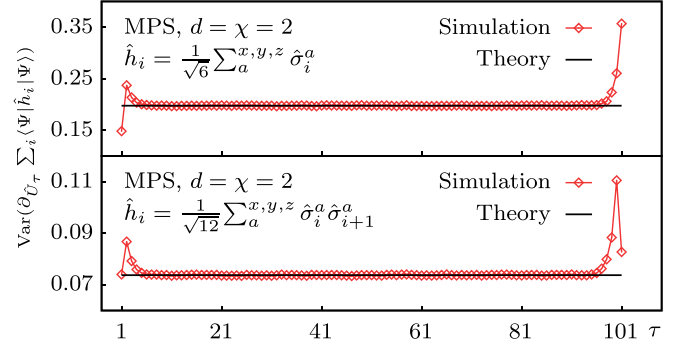


FIG. 2. MPS gradient variance. For spin-1/2 chains (1) of length $L = 101$ with single-site terms $\hat{h}_i = \sum_a \hat{\sigma}_i^a / \sqrt{6}$ (upper panel) and nearest-neighbor interactions $\hat{h}_i = \sum_a \hat{\sigma}_i^a \hat{\sigma}_{i+1}^a / \sqrt{12}$ (lower panel), we plot the gradient variance (8) for the tensor at site τ . Numerical averages over 64 000 MPS with tensors sampled according to the Haar measure agree with the analytical results (16) and (17).

state \hat{r}_1 and the first excitation \hat{r}_2 . The repeated application of $\mathcal{E}_{\text{mps}}^{(2)}$ in Eq. (12) quickly converges to \hat{r}_1 . Similarly, its application in Eq. (13) would converge to the corresponding left eigenoperator $\hat{\ell}_1 = \mathbb{1}_{\chi^2}$, but one finds that this does not contribute to the gradient variance. It is the subleading term $\propto \eta_{\text{mps}}^{\tau-i} \hat{\ell}_2$ that ultimately yields

$$\frac{\text{Avg} \text{Tr} (\hat{g}_\tau^{(i)\dagger} \hat{g}_\tau^{(i)})}{\chi d} = \frac{2 \text{Tr}(\hat{h}^2)}{d(\chi^2 d + 1)} \eta_{\text{mps}}^{\tau-i} + O(\eta_{\text{mps}}^{L-i}). \quad (15)$$

Finally, the gradient variance (8) for the extensive Hamiltonian is obtained by summing the contributions (15) for all $i \leq \tau$, resulting in the system-size independent value

$$\text{Var} \left(\partial_{\hat{U}_\tau} \sum_i \langle \Psi | \hat{h}_i | \Psi \rangle \right) = 2 \text{Tr}(\hat{h}^2) \frac{\chi^2 d^2 - 1}{d(d-1)(\chi^2 d + 1)^2} + O(\eta_{\text{mps}}^\tau) + O(\eta_{\text{mps}}^{L-\tau}), \quad (16)$$

where the subleading terms are due to boundary effects.

The optimization problem with single-site terms \hat{h}_i is trivially solved by product states [62]. In contrast, ground-state problems with finite-range interactions \hat{h}_i are quantum-Merlin-Arthur complete [63–67]. Fortunately, the analysis does not change qualitatively for such Hamiltonians. The second largest eigenvalue η_{mps} of the doubled transition channel (14) remains the most important quantity. Specifically, for nearest-neighbor interactions with $\hat{h}_i = \mathbb{1}_d^{\otimes(i-1)} \otimes \hat{h} \otimes \mathbb{1}_d^{\otimes(L-i-1)}$ acting nontrivially on sites i and $i+1$, and assuming large χ , we find

$$\text{Var} \left(\partial_{\hat{U}_\tau} \sum_i \langle \Psi | \hat{h}_i | \Psi \rangle \right) \sim \frac{4}{\chi^2 d^4} [\text{Tr}(\hat{h}^2) + 2 \text{Tr}(\text{Tr}_1^2 \hat{h})] + O(\eta_{\text{mps}}^j) + O(\eta_{\text{mps}}^{L-j}). \quad (17)$$

A detailed derivation is given in the companion paper [68]. Figure 2 confirms the analytical prediction in numerical tests for spin-1/2 chains. Thus, MPS optimizations have *no* barren plateaus for extensive Hamiltonians.

Hierarchical TNS. MERA [48–50] are hierarchical TNS. Starting on \mathcal{N} sites, in each renormalization step $\tau-1 \rightarrow \tau$,

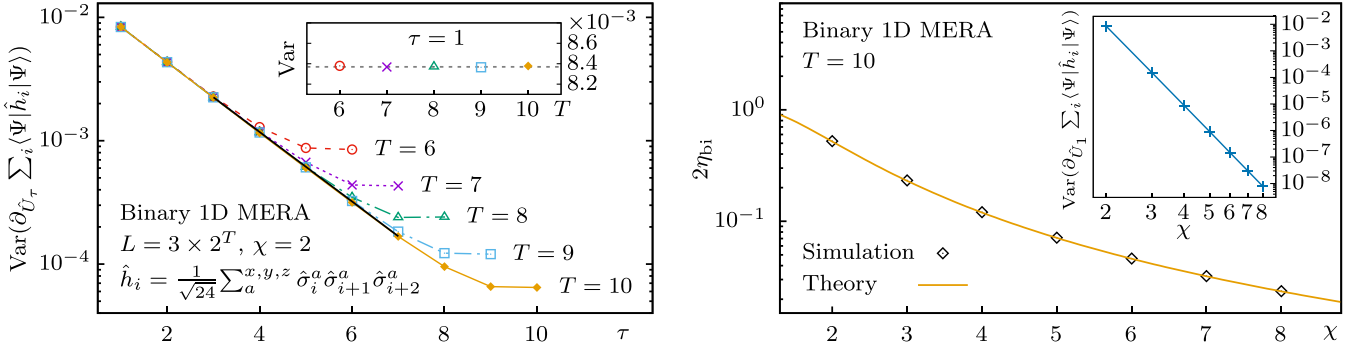


FIG. 3. Gradient variance in heterogeneous 1D MERA. In the hierarchical isometric TNS, the leading term in the Haar variance of the energy gradient (20) is system-size independent and decreases exponentially in the layer index τ . Left: Numerical confirmation for binary 1D MERA with bond dimension $\chi = 2$. The inset shows the variance at $\tau = 1$ as a function of the number of layers $T \lesssim \log_2 L$. Right: Agreement of the decay factors, determined for various bond dimensions χ , and the theoretical prediction $b\eta_{\text{bi}}$. The inset asserts the power-law decay of gradient variances in layer $\tau = 1$ with respect to χ .

we apply local unitary disentangles $\hat{U}_{\tau,k}^\dagger$ of layer τ before the number of degrees of freedom is reduced by applying projections $\hat{V}_{\tau,k}^\dagger$, each mapping a group of b sites into one renormalized site. The dimension χ for the Hilbert space of each renormalized site is the bond dimension and b is the branching ratio. The process stops at the top layer $\tau = T$ by projecting each of the remaining \mathcal{N}/b^T sites onto a reference state $|0_\chi\rangle$. The renormalization procedure, seen in reverse, prepares the MERA $|\Psi\rangle$ starting in layer $\tau = T$ with the reference states $|0_\chi\rangle$ and then proceeding down until reaching the physical layer $\tau = 0$. TTNS [43–47] are a subclass of MERA without disentangles ($\hat{U}_{\tau,k} = \mathbb{1}$).

As all tensors are isometric, the evaluation of local expectation values can be drastically simplified because $\langle \Psi | \hat{h}_i | \Psi \rangle$ only depends on the tensors in the causal cone of \hat{h}_i . See Fig. 1. In fact, the expectation value can again be written in a form very similar to Eq. (10), but now we have transition maps $\mathcal{M}_{\tau,i}$ that map the causal-cone density operator $\hat{\rho}_{\tau,i}$, representing the state on the n_c renormalized sites in the causal cone after preparation steps $T \rightarrow T-1 \rightarrow \dots \rightarrow \tau$, into

$$\hat{\rho}_{\tau-1,i} = \mathcal{M}_{\tau,i}(\hat{\rho}_{\tau,i}) = \mathcal{M}_{\tau,i} \circ \dots \circ \mathcal{M}_{T,i}(|0_\chi\rangle\langle 0_\chi|)^{\otimes n_c}.$$

Specifically, for the binary one-dimensional (1D) MERA in Fig. 1(d) and a three-site interaction term \hat{h}_i , we start at the top layer with the ($n_c = 3$)-site reference state $\hat{\rho}_{T,i} = (|0_\chi\rangle\langle 0_\chi|)^{\otimes 3}$ and then progress down layer by layer, applying either a left-moving or a right-moving transition map $\mathcal{M}_{\tau,i}$: One applies three isometries $\hat{V}_{\tau,k} \otimes \hat{V}_{\tau,k+1} \otimes \hat{V}_{\tau,k+2}$ that double the number of (renormalized) sites to six, then applies two disentangles $\mathbb{1}_\chi \otimes \hat{U}_{\tau,k} \otimes \hat{U}_{\tau,k+1} \otimes \mathbb{1}_\chi$, and, finally, traces out one site on the left and two on the right (left-moving) or vice versa (right-moving).

The diagonal contributions to the gradient variance for $\hat{U}_{\tau,k}$ with $i_1 = i_2 = i$ in Eq. (8) are linear functions of $\text{Avg} \hat{X}_{\tau,k}^{(i)} \otimes \hat{X}_{\tau,k}^{(i)}$ and $\text{Avg} \hat{Y}_{\tau,k}^{(i)} \otimes \hat{Y}_{\tau,k}^{(i)}$, where the additional label k identifies the specific tensor in layer τ . Taking the Haar average of $\mathcal{M}_{\tau,i}^{\otimes 2}$, we obtain a left-moving or right-moving doubled layer-transition channel $\mathcal{E}_{\text{bi,L}}^{(2)}$ and $\mathcal{E}_{\text{bi,R}}^{(2)}$. Summing over all sites $i \in \mathcal{S}_{\tau,k}$ that have $\hat{U}_{\tau,k}$ in their causal cone, corresponds to summing over all possible sequences of the two channels. This is equivalent to applying the map $2\mathcal{E}_{\text{bi}}^{(2)}$ for layers

$t = 1, \dots, \tau - 1$, where

$$\mathcal{E}_{\text{bi}}^{(2)} := \frac{1}{2}(\mathcal{E}_{\text{bi,L}}^{(2)} + \mathcal{E}_{\text{bi,R}}^{(2)}) \quad (18)$$

is the average transition channel. Finally, averaging the gradient variance $\text{Var} \hat{g}(\hat{U}_{\tau,k})$ with respect to k in layer τ corresponds to applying $\mathcal{E}_{\text{bi}}^{(2)}$ for all layers $t = \tau + 1, \dots, T$.

The channel $\mathcal{E}_{\text{bi}}^{(2)}$ is diagonalizable and gapped,

$$\mathcal{E}_{\text{bi}}^{(2)} = |\hat{\ell}_1\rangle\langle\hat{\ell}_1| + \sum_{n=2}^4 \lambda_n |\hat{\ell}_n\rangle\langle\hat{\ell}_n| \quad \text{with} \quad (19)$$

$$\hat{\ell}_1 = \mathbb{1}_{\chi^6}, \quad \eta_{\text{bi}} := \lambda_2 = \frac{\chi^2(1+\chi)^4}{2(1+\chi^2)^4}, \quad \lambda_3 = \frac{\chi^2(1+\chi)^2}{2(1+\chi^2)^3},$$

biorthogonal left and right eigenvectors $\langle\langle \hat{\ell}_n | \hat{\rho}_{\tau,i} \rangle\rangle = \delta_{n,n'}$, and $\frac{1}{2} > \lambda_2 > \lambda_3 > \lambda_4$. Similar to the analysis for MPS, the leading term in $\text{Avg} \hat{X}_{\tau,k}^{(i)} \otimes \hat{X}_{\tau,k}^{(i)}$ stems from the $\mathcal{E}_{\text{bi}}^{(2)}$ steady state $\hat{\rho}_1$, while the leading contributing term in $\text{Avg} \hat{Y}_{\tau,k}^{(i)} \otimes \hat{Y}_{\tau,k}^{(i)}$ stems from the first excitation $\hat{\ell}_2$. It follows that the diagonal contributions to the gradient variance $\text{Var} \partial_{\hat{U}_{\tau,k}} \langle \Psi | \hat{H} | \Psi \rangle$ [Eq. (8)], averaged for all k in layer τ , scale as

$$\text{Var} \hat{g}(\hat{U}_\tau) = \Theta((2\eta_{\text{bi}})^\tau) + O((2\lambda_3)^\tau) + O(2^\tau \eta_{\text{bi}}^\tau), \quad (20)$$

where the Landau symbol $\Theta(f)$ indicates that there exist upper and lower bounds scaling like f . The off-diagonal terms with $|i_1 - i_2| > 3$ vanish due to $\text{Tr} \hat{h}_i = 0$ and the remaining off-diagonal terms have the same scaling as the diagonal terms. See Ref. [68] for details.

The analysis for the binary 1D MERA can be extended to all MERA and TTNS. The central object in the evaluation of their Haar-averaged gradient variances are doubled layer-transition channels $\mathcal{E}^{(2)}$. The gradient variance for tensors in layer τ will then scale as $(b\eta)^\tau$, where η is the second largest $\mathcal{E}^{(2)}$ eigenvalue. This eigenvalue decreases algebraically with increasing bond dimension χ . Specifically, we find

$$\eta = \frac{\chi}{1+\chi^2} \quad \text{for binary 1D TTNS}, \quad (21a)$$

$$\eta = \frac{1}{3\chi^2} + O(\chi^{-4}) \quad \text{for ternary 1D MERA}, \quad (21b)$$

$$\eta = \frac{\chi^2}{1 + \chi^2 + \chi^4} \quad \text{for ternary 1D TTNS, and} \quad (21c)$$

$$\eta = \frac{1}{9\chi^8} + O(\chi^{-10}) \quad \text{for nonary 2D MERA [72].} \quad (21d)$$

So, for each layer τ , the gradient variance is an algebraic function of the bond dimension χ and, up to subleading corrections, independent of the total system size. Therefore, the optimization of hierarchical TNS is *not* hampered by barren plateaus.

For the 1D hierarchical TNS and Hamiltonians with two-site and three-site interactions \hat{h}_i , these analytical results are tested and confirmed numerically as shown in Fig. 3. We choose the physical single-site dimension d equal to χ . The isotropic interaction terms \hat{h}_i are constructed using generalized $\chi \times \chi$ Gell-Mann matrices $\{\hat{\Lambda}^1, \hat{\Lambda}^2, \dots, \hat{\Lambda}^{\chi^2-1}\}$ [73,74], defining m -site interactions as

$$\hat{h}_i = \frac{1}{\sqrt{2^m(\chi^2-1)}} \sum_{a=1}^{\chi^2-1} \hat{\Lambda}_i^a \otimes \dots \otimes \hat{\Lambda}_{i+m-1}^a, \quad (22)$$

which are traceless, have vanishing partial traces, and are normalized according to $\text{Tr}(\hat{h}_i^2) = 1$. Each data point in Fig. 3 corresponds to 1000 TNS with all tensors sampled according to the Haar measure. The numerical results confirm the scaling $(b\eta)^\tau$ with corrections at small τ and small $T - \tau$. The extracted decay factors $b\eta$ display the expected χ dependence in accordance with Eqs. (19) and (21). See the Supplemental Material [75] for further simulation results.

Homogeneous and Trotterized MERA and TTNS. So far we only considered heterogeneous TNS, where all tensors can vary freely. To save computational resources, one can work with homogeneous TNS where, in the case of MERA and TTNS, all equivalent disentanglers and isometries of a given layer τ are identical. In the case of the binary MERA, we can, for example, set $\hat{U}_{\tau,k} \equiv \hat{U}_\tau$ and $\hat{V}_{\tau,k} \equiv \hat{V}_\tau$ for all disentanglers and isometries in layer τ . The theoretical analysis of gradient variances for homogeneous TNS is more involved as it requires higher-moment Haar-measure integrals. Numerical results shown in Fig. 4 establish that they have considerably larger gradient variances than the corresponding heterogeneous states. This is consistent with findings in Refs. [76,77] for other classes of states.

Isometric TNS can be implemented on quantum computers, but it is advisable to impose a substructure for the TNS tensors to reduce costs and achieve a quantum advantage. Specifically, in Trotterized MERA [52,57,78–80], each tensor is constructed as a brickwall circuit with n (Trotter) steps. A generic full MERA can be recovered by increasing n . Figure 4 compares gradient variances for homogeneous Trotterized MERA and full MERA as well as those for Trotterized and full TTNS. The data for three-site interactions (22) show that Trotterized TNS feature larger gradient variances than full TNS, and the first converge to the second as the number n of Trotter steps increases.

Discussion. The presented results substantiate that the considered isometric TNS generally feature *no* barren plateaus in the energy optimization for extensive models with finite-range interactions. This opens a route to efficiently solve

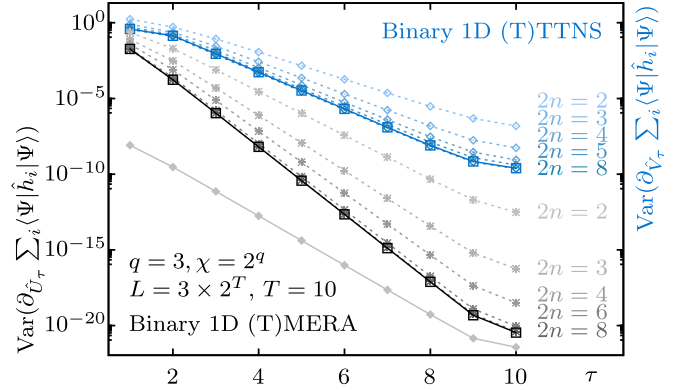


FIG. 4. Gradient variances for homogeneous Trotterized TNS. For the model (22), the plot shows the gradient variances at layer τ for homogeneous binary 1D Trotterized TTNS (blue dashed lines), full TTNS (blue full line), Trotterized MERA (gray dashed lines), and full MERA (black full line), where n denotes the number of Trotter steps per tensor [52,57]. The gray full line shows data for the *heterogeneous* full MERA.

ground-state problems for strongly correlated condensed matter systems with VQA on small quantum computers, e.g., using Trotterized MERA [52,57,79]. For this approach, the benchmark data in Refs. [52,57] imply polynomial quantum advantages which will strongly increase with increasing number of spatial dimensions. In this way, limitations due to high classical tensor contractions costs could be overcome. First experiments demonstrated critical correlations in pre-optimized Trotterized 1D MERA [80].

The observed scaling of the gradient variance has implications for efficient initialization schemes in quantum and classical algorithms: For MPS, the power-law decay in χ suggests to start with an optimization at small χ and to then gradually increase it. For TTNS and MERA, the exponential decay in the layer index τ , suggests that iteratively increasing the number of layers during optimization can substantially improve the performance. TTNS have considerably larger gradient variances than MERA. For MERA optimizations, it can hence be beneficial to initially choose all disentanglers as identities and only start their optimization after the corresponding TTNS has converged.

For VQA with broader classes of quantum circuits, our results suggests that isometric TNS might be a good starting point. One can start with a well-optimized TNS and, subsequently, gradually introduce further quantum gates, which can extend the expressiveness beyond what is achievable in classical simulations without compromising trainability [15,81].

Our results can be generalized to systems with arbitrary finite-range and, more generally, k -local interactions. The proof technique employed in this work, which is centered around the analysis of the doubled (layer or site) transition quantum channels, could also be applied to study statistical properties and typicality for random TNS [82–84], as well as the dynamics of quantum information and entanglement in structured random quantum circuits [85–89].

Acknowledgments. We gratefully acknowledge discussions with K. R. Brown, D. S. França, J.-G. Liu, and I. Marvian as well as support through U.S. Department of

Energy Grant No. DE-SC0019449 and the U.S. National Science Foundation (NSF) Quantum Leap Challenge Institute for Robust Quantum Simulation (Award No. OMA-2120757).

-
- [1] R. P. Feynman, Simulating physics with computers, *Int. J. Theor. Phys.* **21**, 467 (1982).
- [2] M. Cerezo, A. Arrasmith, R. Babbush, S. C. Benjamin, S. Endo, K. Fujii, J. R. McClean, K. Mitarai, X. Yuan, L. Cincio, and P. J. Coles, Variational quantum algorithms, *Nat. Rev. Phys.* **3**, 625 (2021).
- [3] B. T. Kiani, S. Lloyd, and R. Maity, Learning unitaries by gradient descent, [arXiv:2001.11897](https://arxiv.org/abs/2001.11897).
- [4] L. Bittel and M. Kliesch, Training variational quantum algorithms is NP-hard, *Phys. Rev. Lett.* **127**, 120502 (2021).
- [5] E. R. Anschuetz, Critical points in quantum generative models, [arXiv:2109.06957](https://arxiv.org/abs/2109.06957).
- [6] E. R. Anschuetz and B. T. Kiani, Quantum variational algorithms are swamped with traps, *Nat. Commun.* **13**, 7760 (2022).
- [7] J. R. McClean, S. Boixo, V. N. Smelyanskiy, R. Babbush, and H. Neven, Barren plateaus in quantum neural network training landscapes, *Nat. Commun.* **9**, 4812 (2018).
- [8] M. Cerezo, A. Sone, T. Volkoff, L. Cincio, and P. J. Coles, Cost function dependent barren plateaus in shallow parametrized quantum circuits, *Nat. Commun.* **12**, 1791 (2021).
- [9] A. Arrasmith, Z. Holmes, M. Cerezo, and P. J. Coles, Equivalence of quantum barren plateaus to cost concentration and narrow gorges, *Quantum Sci. Technol.* **7**, 045015 (2022).
- [10] Q. Miao and T. Barthele, Equivalence of cost concentration and gradient vanishing for quantum circuits: an elementary proof in the Riemannian formulation, [arXiv:2402.07883](https://arxiv.org/abs/2402.07883).
- [11] E. Grant, L. Wossnig, M. Ostaszewski, and M. Benedetti, An initialization strategy for addressing barren plateaus in parametrized quantum circuits, *Quantum* **3**, 214 (2019).
- [12] K. Zhang, L. Liu, M.-H. Hsieh, and D. Tao, Escaping from the barren plateau via Gaussian initializations in deep variational quantum circuits, [arXiv:2203.09376](https://arxiv.org/abs/2203.09376).
- [13] A. A. Mele, G. B. Mbeng, G. E. Santoro, M. Collura, and P. Torta, Avoiding barren plateaus via transferability of smooth solutions in a Hamiltonian variational ansatz, *Phys. Rev. A* **106**, L060401 (2022).
- [14] A. Kulshrestha and I. Safro, BEINIT: Avoiding barren plateaus in variational quantum algorithms, [arXiv:2204.13751](https://arxiv.org/abs/2204.13751).
- [15] J. Dborin, F. Barratt, V. Wimalaweera, L. Wright, and A. G. Green, Matrix product state pre-training for quantum machine learning, *Quantum Sci. Technol.* **7**, 035014 (2022).
- [16] A. Skolik, J. R. McClean, M. Mohseni, P. van der Smagt, and M. Leib, Layerwise learning for quantum neural networks, *Quantum Mach. Intell.* **3**, 5 (2021).
- [17] L. Slattery, B. Villalonga, and B. K. Clark, Unitary block optimization for variational quantum algorithms, *Phys. Rev. Res.* **4**, 023072 (2022).
- [18] T. Haug and M. S. Kim, Optimal training of variational quantum algorithms without barren plateaus, [arXiv:2104.14543](https://arxiv.org/abs/2104.14543).
- [19] S. H. Sack, R. A. Medina, A. A. Michailidis, R. Kueng, and M. Serbyn, Avoiding barren plateaus using classical shadows, *PRX Quantum* **3**, 020365 (2022).
- [20] A. Rad, A. Seif, and N. M. Linke, Surviving the barren plateau in variational quantum circuits with Bayesian learning initialization, [arXiv:2203.02464](https://arxiv.org/abs/2203.02464).
- [21] Z. Tao, J. Wu, Q. Xia, and Q. Li, LAWS: Look around and warm-start natural gradient descent for quantum neural networks, [arXiv:2205.02666](https://arxiv.org/abs/2205.02666).
- [22] E. Campos, A. Nasrallah, and J. Biamonte, Abrupt transitions in variational quantum circuit training, *Phys. Rev. A* **103**, 032607 (2021).
- [23] C. Dankert, R. Cleve, J. Emerson, and E. Livine, Exact and approximate unitary 2-designs and their application to fidelity estimation, *Phys. Rev. A* **80**, 012304 (2009).
- [24] F. G. S. L. Brandão, A. W. Harrow, and M. Horodecki, Local random quantum circuits are approximate polynomial-designs, *Commun. Math. Phys.* **346**, 397 (2016).
- [25] A. W. Harrow and S. Mehraban, Approximate unitary t -designs by short random quantum circuits using nearest-neighbor and long-range gates, *Commun. Math. Phys.* **401**, 1531 (2023).
- [26] S. Sim, P. D. Johnson, and A. Aspuru-Guzik, Expressibility and entangling capability of parameterized quantum circuits for hybrid quantum-classical algorithms, *Adv. Quantum Technol.* **2**, 1900070 (2019).
- [27] K. Nakaji and N. Yamamoto, Expressibility of the alternating layered ansatz for quantum computation, *Quantum* **5**, 434 (2021).
- [28] Y. Du, Z. Tu, X. Yuan, and D. Tao, Efficient measure for the expressivity of variational quantum algorithms, *Phys. Rev. Lett.* **128**, 080506 (2022).
- [29] Z. Holmes, K. Sharma, M. Cerezo, and P. J. Coles, Connecting ansatz expressibility to gradient magnitudes and barren plateaus, *PRX Quantum* **3**, 010313 (2022).
- [30] S. Goldstein, J. L. Lebowitz, R. Tumulka, and N. Zanghi, Canonical typicality, *Phys. Rev. Lett.* **96**, 050403 (2006).
- [31] S. Popescu, A. J. Short, and A. Winter, Entanglement and the foundations of statistical mechanics, *Nat. Phys.* **2**, 754 (2006).
- [32] C. Ortiz Marrero, M. Kieferová, and N. Wiebe, Entanglement-induced barren plateaus, *PRX Quantum* **2**, 040316 (2021).
- [33] T. L. Patti, K. Najafi, X. Gao, and S. F. Yelin, Entanglement devised barren plateau mitigation, *Phys. Rev. Res.* **3**, 033090 (2021).
- [34] K. Sharma, M. Cerezo, L. Cincio, and P. J. Coles, Trainability of dissipative perceptron-based quantum neural networks, *Phys. Rev. Lett.* **128**, 180505 (2022).
- [35] U. Schollwöck, The density-matrix renormalization group in the age of matrix product states, *Ann. Phys. (NY)* **326**, 96 (2011).
- [36] T. Barthele, J. Lu, and G. Friesecke, On the closedness and geometry of tensor network state sets, *Lett. Math. Phys.* **112**, 72 (2022).
- [37] R. J. Baxter, Dimers on a rectangular lattice, *J. Math. Phys.* **9**, 650 (1968).
- [38] L. Accardi, Topics in quantum probability, *Phys. Rep.* **77**, 169 (1981).

- [39] M. Fannes, B. Nachtergaele, and R. F. Werner, Finitely correlated states on quantum spin chains, *Commun. Math. Phys.* **144**, 443 (1992).
- [40] S. R. White, Density matrix formulation for quantum renormalization groups, *Phys. Rev. Lett.* **69**, 2863 (1992).
- [41] S. Rommer and S. Östlund, A class of ansatz wave functions for 1D spin systems and their relation to DMRG, *Phys. Rev. B* **55**, 2164 (1997).
- [42] D. Perez-Garcia, F. Verstraete, M. M. Wolf, and J. I. Cirac, Matrix product state representations, *Quantum Info. Comput.* **7**, 401 (2007).
- [43] M. Fannes, B. Nachtergaele, and R. F. Werner, Ground states of VBS models on cayley trees, *J. Stat. Phys.* **66**, 939 (1992).
- [44] H. Otsuka, Density-matrix renormalization-group study of the spin-1/2 XXZ antiferromagnet on the Bethe lattice, *Phys. Rev. B* **53**, 14004 (1996).
- [45] Y.-Y. Shi, L.-M. Duan, and G. Vidal, Classical simulation of quantum many-body systems with a tree tensor network, *Phys. Rev. A* **74**, 022320 (2006).
- [46] V. Murg, F. Verstraete, O. Legeza, and R. M. Noack, Simulating strongly correlated quantum systems with tree tensor networks, *Phys. Rev. B* **82**, 205105 (2010).
- [47] L. Tagliacozzo, G. Evenbly, and G. Vidal, Simulation of two-dimensional quantum systems using a tree tensor network that exploits the entropic area law, *Phys. Rev. B* **80**, 235127 (2009).
- [48] G. Vidal, Entanglement renormalization, *Phys. Rev. Lett.* **99**, 220405 (2007).
- [49] G. Vidal, Class of quantum many-body states that can be efficiently simulated, *Phys. Rev. Lett.* **101**, 110501 (2008).
- [50] T. Barthel, M. Kliesch, and J. Eisert, Real-space renormalization yields finitely correlated states, *Phys. Rev. Lett.* **105**, 010502 (2010).
- [51] G. Evenbly, A practical guide to the numerical implementation of tensor networks I: Contractions, decompositions, and gauge freedom, *Front. Appl. Math. Stat.* **8**, 806549 (2022).
- [52] Q. Miao and T. Barthel, Quantum-classical eigensolver using multiscale entanglement renormalization, *Phys. Rev. Res.* **5**, 033141 (2023).
- [53] J.-G. Liu, Y.-H. Zhang, Y. Wan, and L. Wang, Variational quantum eigensolver with fewer qubits, *Phys. Rev. Res.* **1**, 023025 (2019).
- [54] M. Foss-Feig, D. Hayes, J. M. Dreiling, C. Figgatt, J. P. Gaebler, S. A. Moses, J. M. Pino, and A. C. Potter, Holographic quantum algorithms for simulating correlated spin systems, *Phys. Rev. Res.* **3**, 033002 (2021).
- [55] D. Niu, R. Haghshenas, Y. Zhang, M. Foss-Feig, G. K.-L. Chan, and A. C. Potter, Holographic simulation of correlated electrons on a trapped-ion quantum processor, *PRX Quantum* **3**, 030317 (2022).
- [56] L. Slattery and B. K. Clark, Quantum circuits for two-dimensional isometric tensor networks, [arXiv:2108.02792](https://arxiv.org/abs/2108.02792).
- [57] Q. Miao and T. Barthel, Convergence and quantum advantage of Trotterized MERA for strongly-correlated systems, [arXiv:2303.08910](https://arxiv.org/abs/2303.08910).
- [58] Z. Liu, L.-W. Yu, L.-M. Duan, and D.-L. Deng, Presence and absence of barren plateaus in tensor-network based machine learning, *Phys. Rev. Lett.* **129**, 270501 (2022).
- [59] R. J. Garcia, C. Zhao, K. Bu, and A. Jaffe, Barren plateaus from learning scramblers with local cost functions, *J. High Energy Phys.* **01** (2023) 090.
- [60] C. Zhao and X.-S. Gao, Analyzing the barren plateau phenomenon in training quantum neural networks with the ZX-calculus, *Quantum* **5**, 466 (2021).
- [61] E. Cervero Martín, K. Plekhanov, and M. Lubasch, Barren plateaus in quantum tensor network optimization, *Quantum* **7**, 974 (2023).
- [62] For a system of L sites, the expectation value $\langle \Psi | \hat{h}_1 \otimes \hat{h}_2 \otimes \dots \otimes \hat{h}_L | \Psi \rangle$ for normalized states Ψ is simply minimized by the tensor product $|\Psi\rangle = |\psi_1\rangle \otimes \dots \otimes |\psi_L\rangle$ of the lowest-eigenvalue eigenstates ψ_i of the single-site Hamiltonians \hat{h}_i . The same holds for sums $\langle \Psi | \sum_{i=1}^L \hat{h}_i | \Psi \rangle$ of single-site Hamiltonians.
- [63] J. Kempe, A. Kitaev, and O. Regev, The complexity of the local Hamiltonian problem, *SIAM J. Comput.* **35**, 1070 (2006).
- [64] R. Oliveira and B. M. Terhal, The complexity of quantum spin systems on a two-dimensional square lattice, *Quantum Info. Comput.* **8**, 900 (2008).
- [65] D. Aharonov, D. Gottesman, S. Irani, and J. Kempe, The power of quantum systems on a line, *Commun. Math. Phys.* **287**, 41 (2009).
- [66] D. Gottesman and S. Irani, The quantum and classical complexity of translationally invariant tiling and Hamiltonian problems, *Theory of Computing* **9**, 31 (2013).
- [67] J. Bausch, T. Cubitt, and M. Ozols, The complexity of translationally invariant spin chains with low local dimension, *Ann. Henri Poincaré* **18**, 3449 (2017).
- [68] T. Barthel and Q. Miao, Absence of barren plateaus and scaling of gradients in the energy optimization of isometric tensor network states, [arXiv:2304.00161](https://arxiv.org/abs/2304.00161).
- [69] M. Hauru, M. Van Damme, and J. Haegeman, Riemannian optimization of isometric tensor networks, *SciPost Phys.* **10**, 040 (2021).
- [70] I. A. Luchnikov, M. E. Krechetov, and S. N. Filippov, Riemannian geometry and automatic differentiation for optimization problems of quantum physics and quantum technologies, *New J. Phys.* **23**, 073006 (2021).
- [71] R. Wiersema and N. Killoran, Optimizing quantum circuits with Riemannian gradient flow, *Phys. Rev. A* **107**, 062421 (2023).
- [72] G. Evenbly and G. Vidal, Algorithms for entanglement renormalization, *Phys. Rev. B* **79**, 144108 (2009).
- [73] G. Kimura, The Bloch vector for N -level systems, *Phys. Lett. A* **314**, 339 (2003).
- [74] R. A. Bertlmann and P. Krammer, Bloch vectors for qudits, *J. Phys. A: Math. Theor.* **41**, 235303 (2008).
- [75] See Supplemental Material at <http://link.aps.org/supplemental/10.1103/PhysRevA.109.L050402>. It compares the analytical prediction for the scaling of energy-gradient amplitudes to numerical simulations for different 1D MERA and TTNS. It also discusses how finite-size effects explain the power-law decay observed in Ref. [53] for MPS.
- [76] T. Volkoff and P. J. Coles, Large gradients via correlation in random parameterized quantum circuits, *Quantum Sci. Technol.* **6**, 025008 (2021).
- [77] A. Pesah, M. Cerezo, S. Wang, T. Volkoff, A. T. Sornborger, and P. J. Coles, Absence of barren plateaus in quantum convolutional neural networks, *Phys. Rev. X* **11**, 041011 (2021).
- [78] I. H. Kim and B. Swingle, Robust entanglement renormalization on a noisy quantum computer, [arXiv:1711.07500](https://arxiv.org/abs/1711.07500).

- [79] R. Haghshenas, J. Gray, A. C. Potter, and G. K.-L. Chan, Variational power of quantum circuit tensor networks, *Phys. Rev. X* **12**, 011047 (2022).
- [80] R. Haghshenas, E. Chertkov, M. DeCross, T. M. Gatterman, J. A. Gerber, K. Gilmore, D. Gresh, N. Hewitt, C. V. Horst, M. Matheny, T. Mengle, B. Neyenhuis, D. Hayes, and M. Foss-Feig, Probing critical states of matter on a digital quantum computer, [arXiv:2305.01650](https://arxiv.org/abs/2305.01650).
- [81] M. S. Rudolph, J. Miller, D. Motlagh, J. Chen, A. Acharya, and A. Perdomo-Ortiz, Synergistic pretraining of parametrized quantum circuits via tensor networks, *Nat. Commun.* **14**, 8367 (2023).
- [82] S. Garnerone, T. R. de Oliveira, and P. Zanardi, Typicality in random matrix product states, *Phys. Rev. A* **81**, 032336 (2010).
- [83] S. Garnerone, T. R. de Oliveira, S. Haas, and P. Zanardi, Statistical properties of random matrix product states, *Phys. Rev. A* **82**, 052312 (2010).
- [84] J. Haferkamp, C. Bertoni, I. Roth, and J. Eisert, Emergent statistical mechanics from properties of disordered random matrix product states, *PRX Quantum* **2**, 040308 (2021).
- [85] A. Nahum, J. Ruhman, S. Vijay, and J. Haah, Quantum entanglement growth under random unitary dynamics, *Phys. Rev. X* **7**, 031016 (2017).
- [86] A. Nahum, S. Vijay, and J. Haah, Operator spreading in random unitary circuits, *Phys. Rev. X* **8**, 021014 (2018).
- [87] T. Zhou and A. Nahum, Emergent statistical mechanics of entanglement in random unitary circuits, *Phys. Rev. B* **99**, 174205 (2019).
- [88] A. C. Potter and R. Vasseur, in *Entanglement in Spin Chains: From Theory to Quantum Technology Applications*, edited by A. Bayat, S. Bose, and H. Johannesson (Springer International Publishing, Cham, Switzerland, 2022), pp. 211–249.
- [89] M. P. Fisher, V. Khemani, A. Nahum, and S. Vijay, Random quantum circuits, *Annu. Rev. Condens. Matter Phys.* **14**, 335 (2023).